A Decision-Supporting Multi-Objective Approach for Vibration-Assisted EDM of HARDOX 500 Using NSGA-II and AHP

Huu Danh Tran
Vinh Long University of Technology Education, 73 Nguyen Hue Street, Vinh Long City 85100, Vietnam
danhth@vlute.edu.vn

Hoang Anh Le
Vinh Long University of Technology Education, 73 Nguyen Hue Street, Vinh Long City 85100, Vietnam
anhlh@vlute.edu.vn

Cong Danh Nguyen
Vinh Long Vocational College, Phu Quoi Street, Vinh Long City 85100, Vietnam
congdanh1104@gmail.com

Van Thanh
East Asia University of Technology, Trinh Van Bo Street, Hanoi City 12000, Vietnam
thanh.dinh@eaut.edu.vn

Tat Loi Mai
Vinh University of Technology Education, 3/2 Street, Vinh City 43109, Vietnam
maitatloi@vuted.edu.vn

Manh Cuong Nguyen
Thai Nguyen University of Technology, 3/2 Street, Tich Luong Ward, Thai Nguyen City 251750, Vietnam
nmcuong@tnut.edu.vn (corresponding author)

Received: 7 August 2025 | Revised: 13 September 2025 | Accepted: 24 September 2025

 DOI: https://doi.org/10.48084/etasr.13933

ABSTRACT

This study presents a multi-objective optimization framework for enhancing the performance of Ultrasonic Vibration-assisted Electrical Discharge Machining (UV-EDM) in processing HARDOX 500 steel. The conflicting objectives of maximizing the Material Removal Rate (*MRR*) and minimizing the surface roughness (*Ra*) were simultaneously addressed using the Non-dominated Sorting Genetic Algorithm II (NSGA-II). A set of Pareto-optimal solutions was obtained, representing the trade-offs between machining efficiency and surface integrity. To facilitate the selection of the most suitable solution based on application-specific priorities, the Analytic Hierarchy Process (AHP) was employed to rank the Pareto solutions using assigned weights for *MRR* and *Ra*. The integration of AHP into the NSGA-II framework provided an effective decision-support tool for identifying the optimal compromise solution. The experimental validation confirmed the reliability of the predicted results, highlighting the potential of the proposed hybrid approach for optimizing UV-EDM of hard-to-machine materials. Furthermore, under the optimized discharge conditions, the application of ultrasonic vibration increased *MRR* by 21.65% compared with non-vibration EDM, while *Ra* increased slightly by 5.81%, remaining within an acceptable machining range. These findings underscore both the reliability of the optimization model and the practical significance of ultrasonic vibration in improving EDM performance.

Keywords-HARDOX 500; Ultrasonic Vibration-assisted EDM (UV-EDM); multi-objective optimization; NSGA-II; AHP; surface roughness; material removal rate; decision-making

I. INTRODUCTION

Electrical Discharge Machining (EDM) is a key non-traditional manufacturing method for machining difficult-to-cut materials, such as HARDOX 500, a wear-resistant steel commonly used in harsh mechanical environments. However, conventional EDM is often limited by low *MRR*, poor surface quality, and ineffective debris evacuation. To overcome these drawbacks, UV-EDM has been proposed and investigated in various configurations to enhance the machining performance [1-3].

The application of ultrasonic vibration, either to the tool, the workpiece, or the dielectric fluid, has demonstrated significant improvements in spark stability, flushing efficiency, and debris removal [4-6]. For instance, longitudinal-torsional ultrasonic vibration suppresses taper and improves drilling efficiency in deep-hole machining [4], while ultrasonic circular vibration applied to micro-EDM electrodes enhances both the surface integrity and hole accuracy [7, 8]. Similarly, ultrasonic vibration leads to smaller recast layers, reduced tool wear, and more uniform spark distribution [9-11].

Numerical and experimental models have been developed to understand the effects of vibration amplitude, frequency, and electrode motion on material removal mechanisms [3, 12-13]. These studies highlighted the importance of synchronized vibration and optimized input parameters to maximize the machining benefits [14-16]. In addition, the fluid behavior under ultrasonic excitation, such as cavitation and bubble collapse, has been analyzed to explain the improved flushing and enhanced dielectric renewal [17, 18].

Powder-mixed EDM (PMEDM) has also been integrated with ultrasonic vibration to achieve synergistic effects, particularly in applications requiring antibacterial surfaces [9], high-aspect-ratio grooves [19], or hybrid near-dry processing conditions [20]. However, few studies have explored these methods specifically for HARDOX 500, despite its industrial relevance.

Optimization-based research has shifted toward multi-objective approaches. For example, the Taguchi and response surface methodologies were employed to optimize MRR and *Ra* in ultrasonic-assisted micro-EDM of titanium alloys [21, 22]. Evolutionary algorithms, such as NSGA-II, have also gained traction in EDM studies due to their capability to generate Pareto fronts representing optimal trade-offs [23, 24]. Nevertheless, most existing work terminates at Pareto set generation without providing a structured decision-making framework to guide the final selection of process parameters.

To address this gap, the integration of Multi-Criteria Decision-Making (MCDM) techniques—particularly AHP—with multi-objective evolutionary algorithms has shown promise [25, 26]. AHP allows the incorporation of expert judgment or application-specific preferences into the selection of the most suitable Pareto-optimal solution, a strategy underexplored in the context of UV-EDM, especially for HARDOX 500.

In summary, although prior research has advanced the understanding of UV-EDM in various materials and configurations [27-31], a comprehensive decision-supported optimization framework that combines NSGA-II and AHP for machining HARDOX 500 is still lacking.

Aiming to optimize the EDM performance on difficult-to-machine materials, authors in [32] applied the MCDM method to identify the optimal input parameters for EDM of 90CrSi tool steel using graphite electrodes, demonstrating the material's effectiveness in balancing *MRR* and surface quality. Meanwhile, authors in [33] explored UV-EDM using copper electrodes, combining NSGA-II, Gaussian Process Regression (GPR), and AHP to optimize and select the best trade-off solution between *MRR* and *Ra*. These contributions underscore the growing relevance of hybrid EDM optimization approaches and validate the integration of evolutionary algorithms with decision-making tools in both conventional and vibration-assisted EDM contexts.

Therefore, the objective of the present study is to develop and implement a hybrid optimization approach that integrates NSGA-II and AHP to simultaneously optimize *MRR* and *Ra* in UV-EDM of HARDOX 500. The proposed method aims to generate a set of non-dominated solutions and systematically identify the most suitable parameter combination based on user-defined criteria. This research contributes not only to the machining of HARDOX 500 but also to broader applications of decision-supported optimization in advanced manufacturing.

II. OPTIMIZATION METHODOLOGY

The current study adopts a two-stage optimization framework that integrates the NSGA-II with the AHP to simultaneously optimize *Ra* and *MRR* in UV-EDM of HARDOX 500. The overall methodology involves (i) building surrogate models using GPR, (ii) generating Pareto-optimal solutions via NSGA-II, and (iii) ranking these solutions using AHP to support final decision-making.

A. Surrogate Modeling Using GPR

Prior to optimization, the experimental data were used to construct surrogate models that approximate the relationship between five input parameters—vibration amplitude (*A*), pulse-on time (T_{on}), pulse-off time (T_{off}), peak current (*IP*), and servo voltage (*SV*)—and the two response variables, *Ra* and *MRR*. GPR was selected due to its capability to capture nonlinear relationships and provide uncertainty estimates.

The MATLAB function fitrgp was used to train two separate GPR models for *Ra* and *MRR*, respectively, with automatic hyperparameter optimization and squared exponential kernel functions. These models serve as the objective functions for the subsequent NSGA-II search process.

B. Multi-Objective Optimization with NSGA-II

The multi-objective optimization process was implemented using a customized version of the NSGA-II algorithm in MATLAB. The cost function was defined as a vector of the

predicted *Ra* and *MRR* values obtained from the trained GPR models:

$$CostFunction = @(x)[predict(gprRa, x), predict(gprMRR, x)];$$

where gprRa and gprMRR are the GPR surrogate models trained to approximate *Ra* and *MRR* as functions of the five process parameters (A, T_{on}, T_{off}, IP, SV). The cost function, thus, returns the predicted values of *Ra* and *MRR* for each candidate solution.

The search space was defined based on the minimum and maximum values of the experimental design matrix. The population was initialized using Latin Hypercube Sampling, and each individual represented a combination of the five input parameters. The optimization goals were to minimize *Ra* and maximize *MRR*, leading to a two-objective Pareto front.

- The optimization process was configured with key algorithmic settings, including a population size of 50, 100 generations, a crossover rate of 0.9, a mutation rate of 0.2, and a mutation step size of 0.02. During each iteration, new offspring were generated using Simulated Binary Crossover (SBX) and Gaussian mutation operators. To maintain solution diversity and ensure effective convergence, dominance-based sorting and crowding distance calculations were applied throughout the evolutionary process. These mechanisms were implemented through the following custom MATLAB subfunctions:
- NonDominatedSortingLocal for ranking
- CalcCrowdingDistanceLocal for diversity preservation
- TournamentSelectionLocal for parent selection
- CrossoverLocal and MutateLocal for generating new candidate solutions

In NSGA-II, new candidate solutions are obtained at each generation by applying two evolutionary operators: (i) SBX, where pairs of parent solutions are selected via tournament selection and recombined to produce offspring, and (ii) Gaussian mutation, where random perturbations are added to some decision variables within their allowed ranges. The offspring solutions are then evaluated using the surrogate models (gprRa and gprMRR), merged with the parent population, and the best individuals are retained through non-dominated sorting and crowding distance for the next generation.

The optimization problem is, therefore, formulated as a bi-objective problem:

$$Minimize\ f_1(x) = R_a(x) \quad (1)$$

$$Maximize\ f_2(x) = MRR(x) \quad (2)$$

where $x = (A, T_{on}, T_{off}, IP, SV)$ represents the decision vector of the process parameters.

C. Decision-Making with AHP

While the NSGA-II algorithm effectively produces a diverse set of non-dominated solutions, it does not provide a single best configuration suited for implementation. To resolve this limitation, the AHP was employed as a decision-support tool to rank and select the most appropriate solution from the Pareto front based on multiple criteria.

In this study, the two conflicting objectives—minimizing *Ra* and maximizing *MRR*—were first normalized to bring them onto a comparable scale. The normalization procedure reflects the directional preferences of each objective:

$$Ra_{norm} = \frac{max\ (Ra) - Ra}{max(Ra) - min\ (Ra)} \quad (3)$$

$$MRR_{norm} = \frac{MRR - min(MRR)}{max(MRR) - min\ (MRR)} \quad (4)$$

where *Ra* and *MRR* denote the predicted values obtained from the surrogate models (gprRa and gprMRR) for each Pareto-optimal solution. In other words, for every candidate solution generated by NSGA-II, the input vector $x = (A, T_{on}, T_{off}, IP, SV)$ is evaluated using the trained GPR models to yield *Ra*(x) and *MRR*(x), which are then normalized according to (1) and (2).

A pairwise comparison matrix was then constructed to reflect the relative importance between the two criteria. In this case, *MRR* was considered twice as important as *Ra*, resulting in the following judgment matrix:

$$A = \begin{bmatrix} 1 & 1/2 \\ 2 & 1 \end{bmatrix} \quad (5)$$

Using eigenvalue decomposition, the priority weight vector was calculated and normalized. The derived weights were: $Ra_{(min)} \approx 0.333$, and $MRR \approx 0.667$.

It should be noted that for a 2×2 pairwise comparison matrix, the principal eigenvalue is exactly equal to the matrix size ($\lambda_{max} = 2$), which yields a Consistency Index (*CI*) of zero. Since the Random Index (*RI*) for $n = 2$ is also zero, the Consistency Ratio (*CR*) is strictly zero. This confirms that the weight assignments ($Ra = 0.333$, $MRR = 0.667$) are fully consistent and therefore acceptable. The pairwise comparison matrix is first used to derive these weights. The normalized weights are then multiplied by the normalized objective values of each Pareto solution to compute the composite AHP score using (6). Based on these scores, the solutions are ranked, and the one with the highest score is selected as the best compromise solution:

$$S_i = w_{Ra} \cdot R_{anorm,i} + w_{MRR} \cdot MRR_{norm,i} \quad (6)$$

The solution with the highest AHP composite score was selected as the optimal compromise solution, striking a balance between machining efficiency and surface quality. This solution was extracted and saved for reproducibility and downstream analysis.

III. EXPERIMENTAL WORK

Figure 1 shows the experimental setup with a Sodick A30 CNC-EDM system, which was modified to incorporate a high-power ultrasonic vibration module. This integration aimed to enhance spark stability, improve dielectric flushing efficiency, and promote more effective debris evacuation during the machining of hard materials.

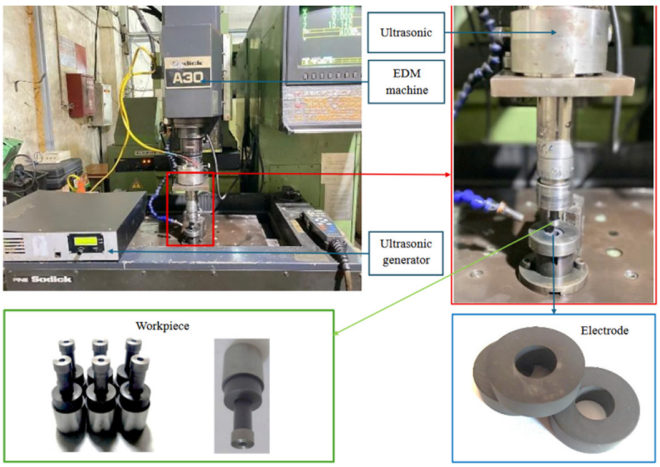

Fig. 1. Experimental setup with a Sodick A30 CNC-EDM system.

Ultrasonic vibrations were generated using an MPI WG-3000 ultrasonic generator (MPI Ultrasonics, Switzerland) with a rated power of 3000 W. These vibrations were transmitted through an RPS-5020-4Z ultrasonic transducer, operating at a frequency of 20 kHz and nominal power of 2000 W. To efficiently transfer the vibratory energy to the machining zone, a custom-fabricated titanium horn was employed. The horn ensured consistent vibratory motion at the tool–workpiece interface, a critical factor for maintaining uniform spark distribution and enhancing the flushing mechanism.

The tool electrode used in this study was composed of HK0 graphite, selected for its excellent electrical conductivity and favorable wear resistance in EDM applications. The dielectric fluid was Diel MS 7000 (Total, France), a commercial EDM oil known for stable discharge behavior and thermal resistance. The workpiece material was HARDOX 500 steel, a hardened alloy with high abrasion resistance. All specimens were cylindrical in geometry to facilitate consistent flushing and surface evaluation.

Two machining performance indicators were considered output responses, including *MRR* and *Ra*. The *MRR* was measured using the gravimetric method, which is widely accepted in EDM research due to its high precision and reproducibility. Before machining, each workpiece was cleaned with ethanol, dried with warm air, and weighed using an analytical balance with a resolution of 0.1 mg. After machining, the same cleaning and drying process was applied before reweighing the sample. The *MRR* (*g*/*h*) was calculated using:

$$MRR = \frac{m_{before} - m_{after}}{t} \times 3600 \quad (7)$$

where m_{before} and m_{after} are the workpiece masses (g) before and after machining, and t is the machining time (s).

The *Ra* of the machined surfaces was measured using a Mitutoyo SV3100 surface roughness tester. To ensure the reliability and representativeness of the measurements, three readings were taken at different positions along the external cylindrical surface of each specimen. The average value of these readings was reported as the final *Ra* for each experiment.

TABLE I. INPUT PARAMETERS AND OUTPUT RESULTS

No	*A* (µm)	T_{on} (µs)	T_{off} (µs)	*IP* (A)	*SV* (V)	*MRR* (g/h)	*Ra* (µm)
1	1.2	8	12	10	5	3.346	3.353
2	1.2	16	12	10	5	1.482	6.569
3	5.2	8	12	10	5	3.119	3.198
4	5.2	16	12	10	5	1.228	5.711
5	3.2	12	8	5	5	1.210	7.220
6	3.2	12	8	15	5	3.665	6.764
7	3.2	12	16	5	5	1.317	6.462
8	3.2	12	16	15	5	4.013	7.260
9	3.2	8	12	10	4	3.293	3.175
10	3.2	8	12	10	6	3.211	3.201
11	3.2	16	12	10	4	1.572	5.889
12	3.2	16	12	10	6	1.416	6.588
13	1.2	12	8	10	5	3.474	5.418
14	1.2	12	16	10	5	3.850	4.492
15	5.2	12	8	10	5	4.073	5.444
16	5.2	12	16	10	5	3.832	4.959
17	3.2	12	12	5	4	1.347	6.339
18	3.2	12	12	5	6	1.274	5.968
19	3.2	12	12	15	4	3.732	6.726
20	3.2	12	12	15	6	4.167	7.312
21	3.2	8	8	10	5	4.216	3.430
22	3.2	8	16	10	5	3.290	3.256
23	3.2	16	8	10	5	1.391	7.280
24	3.2	16	16	10	5	1.360	5.313
25	1.2	12	12	5	5	1.351	6.730
26	1.2	12	12	15	5	3.943	7.595
27	5.2	12	12	5	5	1.243	6.099
28	5.2	12	12	15	5	3.993	8.799
29	3.2	12	8	10	4	4.010	5.790
30	3.2	12	8	10	6	4.069	5.019
31	3.2	12	16	10	4	4.046	5.287
32	3.2	12	16	10	6	4.041	5.479
33	1.2	12	12	10	4	3.759	4.408
34	1.2	12	12	10	6	3.746	5.259
35	5.2	12	12	10	4	3.853	6.312
36	5.2	12	12	10	6	3.811	5.564
37	3.2	8	12	5	5	1.444	2.965
38	3.2	8	12	15	5	3.364	3.850
39	3.2	16	12	5	5	0.969	7.694
40	3.2	16	12	15	5	1.566	12.089
41	3.2	12	12	10	5	3.733	4.483
42	3.2	12	12	10	5	3.829	4.919
43	3.2	12	12	10	5	3.822	5.483
44	3.2	12	12	10	5	3.799	5.032
45	3.2	12	12	10	5	3.764	5.455
46	3.2	12	12	10	5	3.775	4.785

The experimental design employed in this study was based on the Box–Behnken Design (BBD), which is well-suited for response surface modeling involving multiple variables while minimizing the number of experimental runs. A total of five input parameters were selected for investigation: vibration amplitude (*A*), pulse-on time (T_{on}), pulse-off time (T_{off}), peak current (*IP*), and servo voltage (*SV*). Each of these factors was varied at three levels (low, medium, and high), with the specific parameter ranges determined through preliminary experiments and bounded by the capabilities of the EDM machine and ultrasonic system.

The complete experimental matrix, along with the measured responses of *MRR* and *Ra* for each run, is summarized in Table I.

IV. RESULTS AND DISCUSSION

A. Model Fidelity and Validation

The accuracy of the surrogate models was first evaluated to ensure their suitability for guiding the subsequent multi-objective optimization. Table II summarizes the performance indicators of the trained GPR models for *Ra* and *MRR*, based on both training data and 5-fold cross-validation.

As presented in Table II, the GPR model for *MRR* demonstrated excellent predictive performance, with R^2 = 0.9889 for training and 0.8742 for cross-validation, together with very low errors (*RMSE* = 0.4117 g/h, *MAPE* = 15.25%). For *Ra*, the surrogate achieved R^2 = 0.9526 on training data but decreased to 0.5947 under cross-validation, with an *RMSE* of 1.0659 µm and a *MAPE* of 12.66%. Despite this reduction in accuracy, the model was still able to capture the overall response trends.

TABLE II. PERFORMANCE INDICATORS OF THE GPR SURROGATE MODELS FOR RA AND MRR

Response	Set	R^2	*RMSE*	*MAE*	$MAPE_{percent}$
Ra	Training	0.9526	0.3645	0.2932	5.38
Ra	5-Fold CV	0.5947	1.0659	0.711	12.66
MRR	Training	0.9889	0.1224	0.1014	4.52
MRR	5-Fold CV	0.8742	0.4117	0.2955	15.25

Figure 2 further illustrates the goodness of fit through the predicted versus the actual plots for both *MRR* and *Ra* in Figures 2(a) and 2(b), respectively. The closer clustering of *MRR* predictions around the 45° reference line confirms the strong reliability of the *MRR* model, while the *Ra* model shows more scatter yet retains acceptable approximation capability. Overall, these results confirm that the surrogate models, particularly for *MRR*, are sufficiently accurate and robust for integration into the NSGA-II optimization procedure.

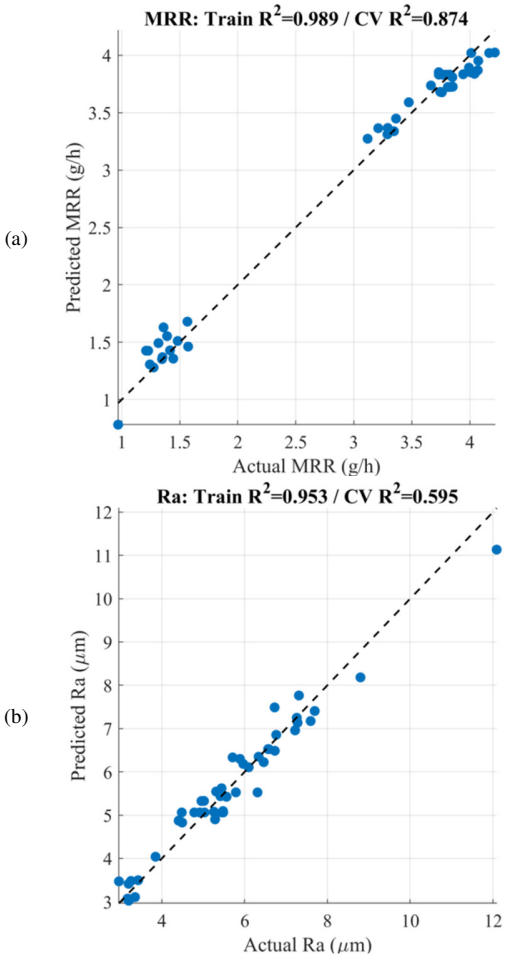

Fig. 2. Predicted versus actual plots for: (a) *MRR* and (b) *Ra*.

B. Pareto Front Analysis and Convergence

Figure 3 displays the final Pareto front obtained by NSGA-II using the GPR surrogates. The front shows the expected inverse relation between productivity and surface integrity: a higher *MRR* is accompanied by a higher *Ra*, whereas a lower *Ra* requires sacrificing *MRR*.

To demonstrate algorithmic stability, Figure 4 provides snapshots of the front at several generations (Gen 1, 30, 70, 100) together with the final front. The cloud rapidly approaches the trade-off curve within the first ~30–70 generations, and then stabilizes with only minor refinements thereafter, indicating that the optimization did not terminate prematurely and that the reported front is representative of the underlying trade-off surface.

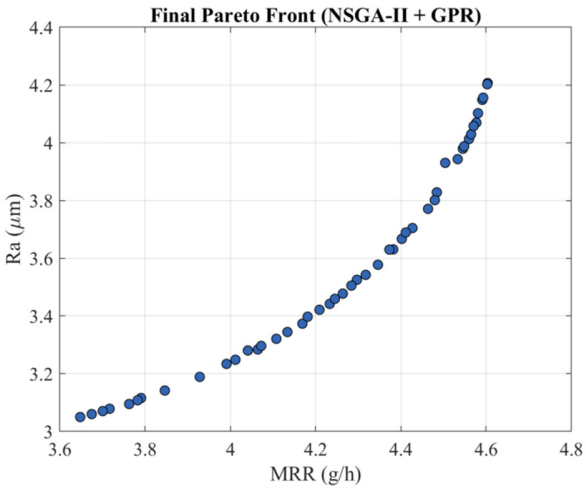

Fig. 3. Final Pareto front of predicted *MRR* versus *Ra*.

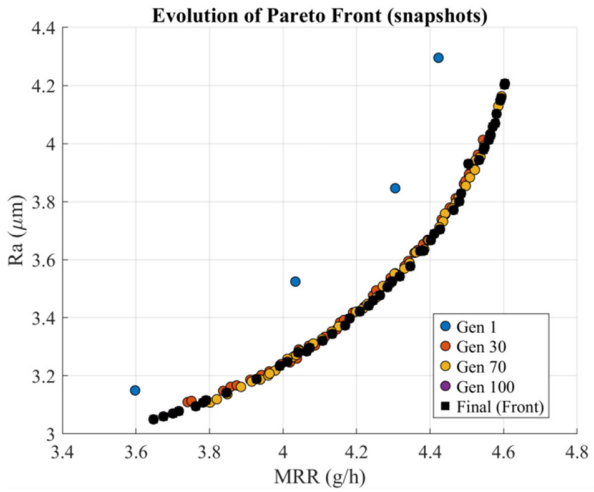

Fig. 4. Evolution of the Pareto front at selected generations (Gen 1, 30, 70, 100) and the final front.

C. Ranking of Pareto Solutions Using AHP

To facilitate decision-making, the 46 Pareto-optimal solutions were evaluated using the AHP. As described earlier, the two objectives—*Ra* and *MRR*—were normalized and assigned weights of 0.333 and 0.667, respectively, reflecting a greater emphasis on productivity.

To enhance interpretability, an AHP ranking graph was generated, as portrayed in Figure 5, showing the AHP scores for all Pareto solutions. From the bar chart, it is evident that the AHP ranking introduces a systematic, preference-guided approach for selecting a final solution from the Pareto front. The best compromise solution, marked in red, offers high *MRR* while maintaining *Ra* within acceptable limits.

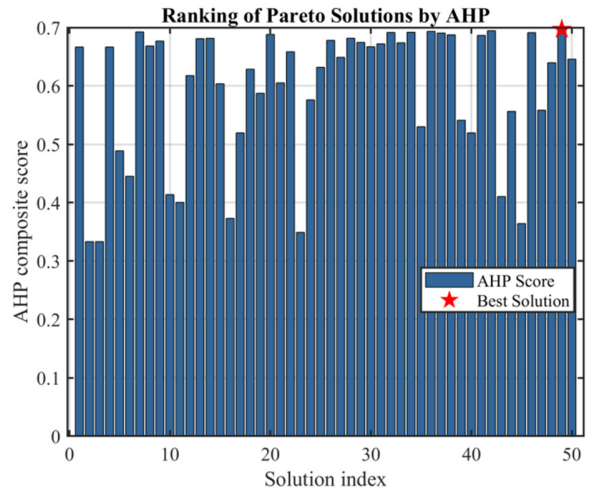

Fig. 5. Ranking of Pareto-optimal solutions based on AHP composite scores. The red marker indicates the best solution.

D. Characteristics of the Optimal Solution

The top-ranked solution identified by AHP was extracted from the optimization results and is summarized in Table III.

TABLE III. PROCESS PARAMETERS AND PREDICTED RESPONSES OF THE BEST AHP-RANKED SOLUTION

Parameter	Value
Vibration amplitude (*A*) (μm)	3.401
Pulse-on time (T_{on}) (μs)	9.040
Pulse-off time (T_{off}) (μs)	8.649
Peak current (*IP*) (A)	11.658
Servo voltage (*SV*) (V)	5.184
Ra (μm)	3.801
MRR (g/h)	4.480

As presented in Table III, the solution achieves an *MRR* of 4.48 g/h, indicating strong machining efficiency, while maintaining an *Ra* of 3.801 μm, which remains within an acceptable range for many engineering applications involving HARDOX 500 steel. The relatively high peak current and moderate vibration amplitude likely contribute to the enhanced material removal performance, while the balanced pulse durations and servo voltage help control the spark stability and surface quality.

This result validates the effectiveness of the proposed NSGA-II + AHP framework in delivering an actionable, preference-guided optimal solution for complex, multi-criteria EDM processes.

E. Experimental Validation of the Optimal Solution and Effect of Ultrasonic Vibration

To assess the reliability of the identified optimal solution, an experiment was conducted using the optimal parameter setting adjusted to the actual CNC machine with: A = 3.4 μm, T_{on} = 9.0 μs, T_{off} = 8.5 μs, IP = 11.6 A, and SV = 5.0 V. The workpiece mass before and after machining was measured using an electronic balance to calculate the *MRR*, while *Ra* was also measured. The experimental results, averaged over three replications, yielded an *MRR* = 4.37 g/h and *Ra* = 3.72 μm. Compared with the model predictions (*MRR* = 4.48 g/h, *Ra* = 3.801 μm), the deviations were 2.46% for MRR and 2.13% for *Ra*. These small errors fall within acceptable limits, confirming the reliability of the optimized model.

In addition, to evaluate the effect of ultrasonic vibration on the EDM process, the same pulse conditions were applied without vibration (A = 0 μm). The experimental results over three replications showed: *MRR* = 3.51 g/h and *Ra* = 3.58 μm. Under the optimized discharge regime, introducing ultrasonic vibration increased *MRR* by 24.5% compared with EDM without vibration. Although *Ra* increased slightly by 3.76% (from 3.58 to 3.72 μm), the resulting value remained within an acceptable machining range. These results demonstrate that ultrasonic vibration provides a significant productivity gain while maintaining *Ra* at an acceptable level.

These validation experiments not only confirm the predictive accuracy of the proposed NSGA-II–AHP optimization framework but also highlight the tangible benefits of incorporating ultrasonic vibration into EDM of HARDOX 500. The significant productivity gain with only a marginal increase in *Ra* underscores the practical applicability of the optimized strategy. These findings provide a solid basis for drawing the final conclusions and implications.

V. CONCLUSION

This study proposed a decision-supported optimization framework for Ultrasonic Vibration-assisted Electrical Discharge Machining (UV-EDM) of HARDOX 500 steel, integrating the Non-dominated Sorting Genetic Algorithm (NSGA-II) multi-objective evolutionary algorithm with the Analytic Hierarchy Process (AHP) to simultaneously optimize Material Removal Rate (*MRR*) and surface roughness (*Ra*).

The key conclusions from this study are:

- The experimental data, collected through a statistically designed Box–Behnken matrix, provided a reliable foundation for modeling the nonlinear relationships between five process parameters (vibration amplitude, pulse-on time, pulse-off time, peak current, and servo voltage) and two critical output responses (*MRR* and *Ra*).
- The Gaussian Process Regression (GPR) surrogate models demonstrated high fidelity in capturing the complex response surfaces, enabling efficient optimization through NSGA-II without the need for excessive experimental runs.
- The NSGA-II algorithm successfully generated a diverse Pareto front of non-dominated solutions, clearly illustrating the trade-off between productivity and surface quality inherent to the UV-EDM process.
- The use of AHP allowed the incorporation of decision-maker preferences—prioritizing *MRR* over *Ra* in this case—and led to the identification of an optimal compromise solution with *MRR* ≈ 4.48 g/h and *Ra* ≈ 3.801 µm.
- The integrated NSGA-II–AHP framework proved to be effective not only in providing a wide range of high-quality solutions but also in selecting the most appropriate one for practical implementation based on specific application needs.
- The validation experiments confirmed the predictive accuracy of the optimal solution and further revealed that ultrasonic vibration increased *MRR* by more than 24% compared with non-vibration EDM under the same discharge conditions, while maintaining *Ra* within an acceptable range—underscoring both the reliability and the practical value of the proposed approach.

ACKNOWLEDGMENT

This work was supported by the Ministry of Education and Training of Vietnam (MOET) through Project B2024-TNA-18.

DATA AVAILABILITY

The dataset used in this study can be available from the corresponding author upon request.

REFERENCES

[1] M. Xu *et al.*, "Ultrasonic and Electrical Discharge–Assisted Milling of the Ti-6Al-4 V Alloy," *The International Journal of Advanced Manufacturing Technology*, vol. 122, no. 3–4, pp. 1897–1917, Sept. 2022, https://doi.org/10.1007/s00170-022-10010-y.

[2] P. Wang *et al.*, "Debris Motion and Taper Suppression in EDM Deep Hole Machining Assisted by Iongitudinal/Torsional Ultrasonic Vibration," *Journal of Manufacturing Processes*, vol. 133, pp. 798–810, Jan. 2025, https://doi.org/10.1016/j.jmapro.2024.11.070.

[3] P. Zhang *et al.*, "Investigating Mechanisms of Debris Removal in Ultrasonic Vibration-Assisted EDM Drilling," *International Journal of Mechanical Sciences*, vol. 279, Oct. 2024, Art. no. 109486, https://doi.org/10.1016/j.ijmecsci.2024.109486.

[4] M. Xu, Z. Wu, F. Gao, L. Liu, and E. Song, "Error Modeling and Accuracy Optimization of Rotating Ultrasonic Vibration Assisted EDM Machine Tool," *Journal of Mechanical Science and Technology*, vol. 34, no. 7, pp. 2751–2760, July 2020, https://doi.org/10.1007/s12206-020-0607-4.

[5] Z. Yin *et al.*, "A novel EDM Method using Longitudinal-torsional Ultrasonic Vibration (LTV) Electrodes to Improve Machining Performance for Micro-holes," *Journal of Manufacturing Processes*, vol. 102, pp. 231–243, Sept. 2023, https://doi.org/10.1016/j.jmapro.2023.07.023.

[6] A. Hirao, H. Gotoh, and T. Tani, "Some Effects on EDM Characteristics by Assisted Ultrasonic Vibration of the Tool Electrode," *Procedia CIRP*, vol. 68, pp. 76–80, 2018, https://doi.org/10.1016/j.procir.2017.12.025.

[7] Z. Li, J. Tang, and J. Bai, "A Novel Micro-EDM Method to Improve Microhole Machining Performances using Ultrasonic Circular vibration (UCV) Electrode," *International Journal of Mechanical Sciences*, vol. 175, June 2020, Art. no. 105574, https://doi.org/10.1016/j.ijmecsci.2020.105574.

[8] Y. Zhang and B. Xie, "Investigation on Hole Diameter Non-uniformity of Hole Arrays by Ultrasonic Vibration-assisted EDM," *The International Journal of Advanced Manufacturing Technology*, vol. 112, no. 11–12, pp. 3083–3091, Feb. 2021, https://doi.org/10.1007/s00170-021-06597-3.

[9] V. D. Bui *et al.*, "Ultrasonic Vibration Assisted Silver Integration by Powder Mixed EDM for Antibacterial Surfaces," *Procedia CIRP*, vol. 123, pp. 410–415, 2024, https://doi.org/10.1016/j.procir.2024.05.072.

[10] Z. Li, J. Tang, Y. Li, and J. Bai, "Investigation on Surface Integrity in Novel Micro-EDM with Two-dimensional Ultrasonic Circular Vibration (UCV) Electrode," *Journal of Manufacturing Processes*, vol. 76, pp. 828–840, Apr. 2022, https://doi.org/10.1016/j.jmapro.2022.03.004.

[11] S. Hou, J. Bai, H. Liu, Z. Zhou, and Z. Lu, "Study on Material Erosion Mechanism of Ultrasonic Vibration-assisted Micro-EDM based on Heat-flow Coupling Analysis," *The International Journal of Advanced Manufacturing Technology*, vol. 125, no. 1–2, pp. 465–478, Mar. 2023, https://doi.org/10.1007/s00170-022-10695-1.

[12] M. Choubey, K. P. Maity, and A. Sharma, "Finite Element Modeling of Material Removal Rate in Micro-EDM Process with and without Ultrasonic Vibration," *Grey Systems: Theory and Application*, vol. 10, no. 3, pp. 311–319, Mar. 2020, https://doi.org/10.1108/GS-11-2019-0047.

[13] M. T. Shervani-Tabar, K. Maghsoudi, and M. R. Shabgard, "Effects of Simultaneous Ultrasonic Vibration of the Tool and the Workpiece in Ultrasonic Assisted EDM," *International Journal for Computational Methods in Engineering Science and Mechanics*, vol. 14, no. 1, pp. 1–9, Jan. 2013, https://doi.org/10.1080/15502287.2012.698696.

[14] D. Kremer, C. Lhiaubet, and A. Moisan, "A Study of the Effect of Synchronizing Ultrasonic Vibrations with Pulses in EDM," *CIRP Annals*, vol. 40, no. 1, pp. 211–214, 1991, https://doi.org/10.1016/S0007-8506(07)61970-2.

[15] M. R. Shabgard, A. Gholipoor, and M. Mohammadpourfard, "Numerical and Experimental Study of the Effects of Ultrasonic Vibrations of Tool on Machining Characteristics of EDM Process," *The International Journal of Advanced Manufacturing Technology*, vol. 96, no. 5–8, pp. 2657–2669, May 2018, https://doi.org/10.1007/s00170-017-1487-3.

[16] M. T. Shervani-Tabar, A. Abdullah, and M. R. Shabgard, "Numerical and Experimental Study on the Effect of Vibration of the Tool in Ultrasonic Assisted EDM," *The International Journal of Advanced Manufacturing Technology*, vol. 32, no. 7–8, pp. 719–731, Mar. 2007, https://doi.org/10.1007/s00170-006-0828-4.

[17] W. Chenxue, T. Sasaki, and A. Hirao, "Observation of Bubble Behavior in EDM with Ultrasonic Vibration," *Procedia CIRP*, vol. 113, pp. 267–272, 2022, https://doi.org/10.1016/j.procir.2022.09.157.

[18] Y. Wang, L. Fan, J. Shi, Y. Dong, and Z. Fu, "Effect of Cavitation on Surface Formation Mechanism of Ultrasonic Vibration-assisted EDM," *The International Journal of Advanced Manufacturing Technology*, vol. 124, no. 10, pp. 3645–3656, Feb. 2023, https://doi.org/10.1007/s00170-022-10780-5.

[19] Q. Xing, M. Gao, Z. Yao, and Q. Zhang, "Research on Ultrasonic Vibration–assisted Micro-EDM Milling of Microgrooves with Large Aspect Ratio," *The International Journal of Advanced Manufacturing Technology*, vol. 128, no. 3–4, pp. 1629–1639, Sept. 2023, https://doi.org/10.1007/s00170-023-11984-z.

[20] M. Li, T. Zhang, L. Fu, L. Ding, and L. Xie, "Research on the Strengthening Layer of TC4 Alloy Strengthened by Ultrasonic Vibration-assisted Powder-mixed Near-dry Multi-dielectrics EDM," *Journal of Mechanical Science and Technology*, vol. 39, no. 3, pp. 1151–1158, Mar. 2025, https://doi.org/10.1007/s12206-025-0211-8.

[21] M. M. Sundaram, G. B. Pavalarajan, and K. P. Rajurkar, "A Study on Process Parameters of Ultrasonic Assisted Micro EDM Based on Taguchi Method," *Journal of Materials Engineering and Performance*, vol. 17, no. 2, pp. 210–215, Apr. 2008, https://doi.org/10.1007/s11665-007-9128-x.

[22] P. Singh, V. Yadava, and A. Narayan, "Parametric Study of Ultrasonic-assisted Hole Sinking Micro-EDM of Titanium Alloy," *The International Journal of Advanced Manufacturing Technology*, vol. 94, no. 5–8, pp. 2551–2562, Feb. 2018, https://doi.org/10.1007/s00170-017-1051-1.

[23] P. Zhang *et al.*, "Experimental Research and Multi-objective Optimization of Ultrasonic Vibration–assisted EDM for Ti6Al4V Micro-holes," *The International Journal of Advanced Manufacturing Technology*, vol. 127, no. 7–8, pp. 3413–3425, Aug. 2023, https://doi.org/10.1007/s00170-023-11641-5.

[24] J. Xu, S. Xia, P. Yu, and M. Li, "Multi-objective Parameter Optimization of Ultrasonic Vibration–assisted Micro-EDM of Ti-6Al-4V Alloys," *Journal of Vibration and Control*, vol. 30, no. 7–8, pp. 1818–1828, Apr. 2024, https://doi.org/10.1177/10775463231171798.

[25] S. Hou and J. Bai, "A Novel Ultrasonic Vibration-assisted Micro-EDM Method to Improve Debris Removal Performance using Relative Three-dimensional Ultrasonic Vibration (RTDUV)," *The International Journal of Advanced Manufacturing Technology*, vol. 127, no. 11–12, pp. 5711–5727, Aug. 2023, https://doi.org/10.1007/s00170-023-11971-4.

[26] Y. Dong *et al.*, "Study on Mechanism and Surface Topography of Ultrasonic Powder Mixing–assisted EDM," *The International Journal of Advanced Manufacturing Technology*, vol. 135, no. 1–2, pp. 337–350, Nov. 2024, https://doi.org/10.1007/s00170-024-14418-6.

[27] Y.-C. Lin, J.-C. Hung, H.-M. Chow, A.-C. Wang, and J.-T. Chen, "Machining Characteristics of a Hybrid Process of EDM in Gas Combined with Ultrasonic Vibration and AJM," *Procedia CIRP*, vol. 42, pp. 167–172, 2016, https://doi.org/10.1016/j.procir.2016.02.213.

[28] M. G. Xu, J. H. Zhang, Y. Li, Q. H. Zhang, and S. F. Ren, "Material Removal Mechanisms of Cemented Carbides Machined by Ultrasonic Vibration Assisted EDM in Gas Medium," *Journal of Materials Processing Technology*, vol. 209, no. 4, pp. 1742–1746, Feb. 2009, https://doi.org/10.1016/j.jmatprotec.2008.04.031.

[29] J. M. Jafferson, P. Hariharan, and J. Ram Kumar, "Effects of Ultrasonic Vibration and Magnetic Field in Micro-EDM Milling of Nonmagnetic Material," *Materials and Manufacturing Processes*, vol. 29, no. 3, pp. 357–363, Mar. 2014, https://doi.org/10.1080/10426914.2013.872268.

[30] Y. Wang *et al.*, "Analysis of Material Removal and Surface Generation Mechanism of Ultrasonic Vibration–assisted EDM," *The International Journal of Advanced Manufacturing Technology*, vol. 110, no. 1–2, pp. 177–189, Sept. 2020, https://doi.org/10.1007/s00170-020-05769-x.

[31] C. Praneetpongrung, Y. Fukuzawa, S. Nagasawa, and K. Yamashita, "Effects of the EDM Combined Ultrasonic Vibration on the Machining Properties of Si3N4," *MATERIALS TRANSACTIONS*, vol. 51, no. 11, pp. 2113–2120, 2010, https://doi.org/10.2320/matertrans.M2010194.

[32] T. P. T. Le, V. T. Dinh, T. Q. D. Nguyen, D. B. Vu, and T. T. Vu, "Application of the Multi-Criteria Decision Method to Find the Best Input Factors for Electrical Discharge Machining 90CrSi Tool Steel using Graphite Electrodes," *Engineering, Technology & Applied Science Research*, vol. 14, no. 6, pp. 18883–18888, Dec. 2024, https://doi.org/10.48084/etasr.9114.

[33] V. T. Dinh, T. Q. Le, T. T. Do, N. P. Vu, and T. P. T. Tran, "Multi-Objective Optimization of Material Removal Rate and Surface Roughness in Ultrasonic Vibration-Assisted EDM Using NSGA-II, GPR, and AHP," *Engineering, Technology & Applied Science Research*, vol. 15, no. 4, pp. 24977–24984, Aug. 2025, https://doi.org/10.48084/etasr.11380.